Article:
Li, LH, Zhu, JX, Chen, L et al. (2 more authors) (2015) The MBE growth and optimization of high performance terahertz frequency quantum cascade lasers. Optics Express, 23 (3). 2720 - 2729. ISSN 1094-4087

https://doi.org/10.1364/OE.23.002720

The MBE growth and optimization of high performance terahertz frequency quantum cascade lasers

L. H. Li,* J. X. Zhu, L. Chen, A. G. Davies, and E. H. Linfield

School of Electronic and Electrical Engineering, University of Leeds, Woodhouse Lane, Leeds LS2 9JT, UK

*l.h.li@leeds.ac.uk

Abstract:

The technique of molecular beam epitaxy has recently been used to demonstrate the growth of terahertz frequency GaAs/AlGaAs quantum cascade lasers (QCL) with Watt-level optical output powers. In this paper, we discuss the critical importance of achieving accurate layer thicknesses and alloy compositions during growth, and demonstrate that precise growth control as well as run-to-run growth reproducibility is possible. We also discuss the importance of minimizing background doping level in maximizing QCL performance. By selecting high-performance active region designs, and optimizing the injection doping level and device fabrication, we demonstrate total optical (two-facet) output powers as high as 1.56 W.

1. Introduction

Terahertz (THz) frequency radiation has many potential applications, ranging from imaging and chemical sensing through to telecommunications [1,2]. However, one of the principal challenges has been to develop compact, low-cost, efficient THz sources. The demonstration of the THz frequency quantum cascade laser (QCL) in 2002 provided a potential solid-state solution [3]. Since then, THz QCLs have developed rapidly, offering frequencies from 1.2 to 5 THz [2]; ultra-broadband (1 THz) operation [4]; working temperatures up to 199.5 K [5]; and peak output powers > 1 W [6].

This rapid development has included implementation of novel waveguide schemes [3,7], continuous improvements in active region designs [2–10], and device realization in the mature GaAs/AlGaAs material system, with material grown by established technologies such as molecular beam epitaxy (MBE). The growth of THz QCLs does, however, remain extremely challenging, owing to the stringent demands for precise control of individual layer thicknesses and alloy compositions, which must be maintained over the, typically, 10 µm thick active regions. Yet, despite the extensive studies of waveguide and active region designs, there have been relatively few reports discussing the actual growth process itself, although insight is provided by [11–15]. An excellent compressive review [16], following the successful demonstration of THz QCLs with record working temperatures, does address the growth in greater detail. But issues such as the achievement of growth reproducibility in THz QCLs still need to be addressed fully.

In this paper, we report our recent successful MBE growth of GaAs/AlGaAs THz QCLs with Watt-level optical output powers. This arose from precise growth layer thickness control, high material quality, and optimization of the device fabrication. Pre-growth calibration and real time monitoring of the THz QCL growth are discussed, with the importance of layer thickness and alloy composition control, as well as the background doping level, emphasized.

2. Growth calibration

It is well known that high-performance THz QCLs can only be obtained when the designed structure is strictly realized. This requires precise control of the layer thicknesses and alloy compositions. We have shown previously that pyrometric spectrometry (kSA BandiT) can be used to calibrate layer thicknesses and alloy compositions through real-time growth rate measurements, with the additional advantage that in situ monitoring can be achieved through the whole of the QCL growth itself [6,15]. The technique allows multiple, successive calibrations, which are achieved by analyzing the pyrometric data acquired from the growth of a thick GaAs layer on AlAs, and vice-versa. In both cases, intensity oscillations resulting from interference effects in the growing semiconductor layer can be monitored as a function of time and wavelength. From such oscillations, GaAs and AlAs growth rates can be calculated using the formula $G = \lambda_0/2nT$ [17,18], where G is the growth rate, T is the time period of intensity oscillations at a specific wavelength (λ_0), and n is the material refractive index at the growth temperature. In this formula, λ_0 is fixed and T can be easily obtained from the oscillation curve. Once n is known, calibration is then straightforward. However, there has been a lack of reported data of the refractive indices of GaAs and AlAs at the THz QCL growth temperature of ~600 °C, especially over the wavelength range of 1000-1400 nm where the oscillation curves are acquired using BandiT pyrometric spectroscopy.

To determine n under these conditions, we grew a set of dedicated samples in which thick $Al_xGa_{1-x}As$ layers and an $Al_xGa_{1-x}As$/InAs superlattice (SPL) were sequentially deposited. The thick $Al_xGa_{1-x}As$ layers were used to acquire oscillation curves, whilst the SPLs were used to determine precisely the $Al_xGa_{1-x}As$ layer thickness (to an accuracy of <0.5%) using ex-situ techniques such as x-ray diffraction measurements. Once the $Al_xGa_{1-x}As$ layer thickness was known, the growth rates could then be calculated allowing n to be obtained at different wavelengths by using

values of T extracted from the oscillation curves (to an accuracy of <0.3%). The experimentally obtained values of n for GaAs and AlAs are summarized in Fig. 1, where n (with an accuracy of better than 1%) is plotted as a function of wavelength in the range 900 to 1400 nm. The inset shows the variation of n with increased Al composition in an AlGaAs layer – n decreases with increasing wavelength. This follows the trend observed in the short wavelength range from 400 nm to 1000 nm in previous studies [19,20], with the refractive index values matching in the range 900 – 1000 nm. At ~1000 nm, n is ~3.78 and ~3.05 for GaAs and AlAs, respectively. The values of n for GaAs and AlAs presented here have been checked in multiple growth campaigns across five years, with a high degree of reproducibility observed. They have also been used successfully for daily pre-growth calibration and real time monitoring of THz QCL growth in our laboratory.

3. Layer thickness control and growth reproducibility

The growth rate drift, arising from consumption of group III materials (Ga and Al), is of key importance for the growth of high performance THz QCLs [16]. When both high operating temperature and high output powers are required, the uniformity of the laser stack (or overall periodicity) is a high priority, and this poses stringent demands on the control of the material growth rates over the whole QCL growth period.

Based on the daily pre-growth calibration data recorded over a typical growth campaign, the dependence of the required cell temperature to achieve a 1 µm/hour growth rate for GaAs is plotted in Fig. 2, as a function of the total deposited GaAs layer thickness in the growth campaign. Each data point corresponds to a single wafer growth. The aluminum data reflecting the required cell temperature to achieve a constant growth rate of 0.176 um/hr, as used for the majority of THz QCL growths, are also shown. These aluminum data points correspond to THz QCL growths during the campaign – other device structures require different aluminum mole fractions, and were grown with another aluminum cell. Here, the cells used are an 85 cc dual-filament gallium cell from Veeco and a 40 cc cold tip conical aluminum cell from VG Semicon. As the total campaign growth thickness increases, the gallium cell temperature has to be increased to maintain a constant growth rate. In contrast, the aluminum cell temperature remains nearly constant in our case, even though there are slight temperature fluctuations. Based on these observations, to ensure precise growth control of individual layer thicknesses/alloy compositions in THz QCLs, it is necessary to compensate for GaAs growth rate drifts, but variation in AlAs growth rate can be neglected. However, it is very hard to predict an exact GaAs drift rate over a given time period, as shown in Fig. 2, making it difficult practically to achieve precise growth rate uniformity.

Pyrometric data, in principle, gives extensive information about the precision of the wafer growth, not only acting as an additional calibration during the growth of the QCL itself, but also providing information about growth rate drift during a structure's growth. In a given time period, the growth rate drift for pure GaAs grown on AlAs can be easily determined. In THz QCLs, the structure is far more complex. However, we still noticed that the GaAs growth rate drift can be indirectly extracted during the THz QCL growth.

For the growth of THz QCLs, $G_{QCL} = G_{GaAs}\cdot(1-x_{QCL})^{-1}$, where G_{GaAs} is the GaAs growth rate; x_{QCL} is the average aluminum mole fraction of the QCL; and, G_{QCL} is the average growth rate of the QCL. $1-x_{QCL}$ depends only weakly on G_{GaAs}. Hence, G_{QCL} is dominated by the changes of G_{GaAs}. For a given THz QCL design, once G_{QCL} is known, G_{GaAs}, as well as its growth rate drift, can therefore be obtained. Growth rate compensation can then be realized more precisely, either during the growth itself or subsequent growths. Figure 3 shows a typical oscillation curve of a THz QCL structure in which growth rate compensation is applied. Theoretical simulation, using a transfer matrix method [19], corresponds very well with the experimental oscillation curve, indicating negligible growth rate drift and implying excellent control of the growth layer thickness as well as the overall periodicity of the QCL.

The growth rate compensation technique, together with calibration of GaAs and AlAs growth rates immediately prior to QCL growth, enables high run-to-run growth reproducibility. X-ray diffraction measurements of two QCLs, with nominally identical structures, were found to only show thickness deviations of ~1% (data not shown) even when ~10 different THz QCLs were grown between these two samples. This confirms that pyrometric spectrometry is a powerful technique for achieving reproducible growth of THz QCLs, and enables run-to-run growth repeatability to be obtained.

4. Development of THz QCL with > 1 W output powers

In order to develop THz QCLs with high output powers, it is also essential to optimize the active region design, the electrical material quality, and the device fabrication.

4.1 Device growth, fabrication and characterization

Having optimized the MBE growth process to achieve accurate calibrations for the gallium and aluminum growth rates, and ensure high growth rate uniformities, dedicated 15 µm-thick unintentionally doped bulk GaAs layers were regularly grown to assess material background doping level. The measurements were performed at room temperature using a Van der Pauw method. Once the background is $< 5 \times 10^{14}$ cm^{-3} (p-type in our case), a series of THz QCL active region designs were grown by solid-source MBE on semi-insulating GaAs substrates. These included: the bound-to-continuum active region design with a single-quantum-well phonon extraction/injection stage presented in

[9] (denoted BTC-RP); the modified BTC-RP design presented in [6] (denoted M-BTC-RP); and, the multiple quantum well design with LO-phonon-assisted interminiband transitions presented in [8] (denoted MQW-LO). The complete QCL structures typically consisted of a 250 nm undoped GaAs buffer layer, a 300 nm undoped $Al_{0.5}Ga_{0.5}As$ etch-stop layer, a 600 nm Si-doped GaAs bottom contact layer (doped at 2×10^{18} cm^{-3} or 3.5×10^{18} cm^{-3}), a thick active region (12 μm for BTC-RP and M- BTC-RP structures, 15 μm for the MQW-LO structure), and a 50 nm heavily Si-doped GaAs top contact layer (5×10^{18} cm^{-3}). Immediately prior to growth, the GaAs and AlAs growth rates were determined using BandiT spectrometry to calibrate the layer thicknesses and aluminum mole fractions [6, 15]. To ensure precise growth layer thickness and run-to-run growth reproducibility, growth rate compensation was also used.

Following growth, the wafers were processed into surface-plasmon ridge waveguide device structures using conventional photolithography and wet chemical etching techniques. Ridges with widths (w) ranging from 145 to 425 μm were formed. To improve heat dissipation, the substrate was thinned down to ~180 μm by wet chemical etching. For characterization, devices were cleaved into Fabry-Perot cavities of different length (L) ranging from 1 to 3 mm, wire bonded and indium-soldered to copper submounts.

The devices were characterized in pulsed mode, with a repetition rate of 10 kHz and a duty cycle of 2%, in a liquid-helium continuous-flow cryostat equipped with 1.5-mm-thick polyethylene windows. The radiation was collected from a single facet and the average power was measured using an absolute terahertz power meter (Thomas Keating), which was butted against the cryostat window. The output power was then calculated from the measured average power and duty cycle. Unlike some earlier reports [7, 8], neither a light-pipe nor a Winston core were used, despite a separation (d) of ~3.5 cm between the power meter and the device facet. Furthermore, no correction for collection efficiency is applied to any of the powers reported in this paper.

4.2 Effects of active region doping and background quality on THz QCL performance

If the material layer thickness/alloy composition can be precisely controlled for a given active region design, then the device optical output power is principally determined by the number of periods in the active region (N_p), and the dynamic range J_{max} - J_{th}. Here, J_{max}, the maximum injection current density, is proportional to the sheet carrier density (n_s) in each active region period, and J_{th}, the threshold current density, is a weak function of n_s owing to free carrier absorption [21]. Intuitively, if n_s and N_p increase, the device optical output power will increase, and this is indeed the case [12, 22]. Figure 4 shows the dependencies of (a) the peak output power and (b) J_{max} and J_{th} on the injector doping level, with data reported from two sets of samples grown with different gallium cells (Ga1 and Ga2). For both sets of samples, the device optical output power, as well as J_{max} and J_{th}, scale almost linearly with increasing injector doping level, which is very similar to that reported in [21,23,24]. There is, however, a marked difference between the performance of THz QCLs grown with Ga1 and Ga2, and this arises from the quality of material produced by the two cells. Ga1 produced extremely high quality material, with very low background impurity levels (background carrier concentration < 1×10^{13}cm^{-3}, p-type) whilst Ga2 was known to be contaminated, producing lower quality compensated material, with higher background impurity levels (and a net background carrier concentration of ~2×10^{14}cm^{-3}, p-type). For samples grown with Ga2, there was only a small increase in output power and J_{max} with active region doping, such that with n_s of ~1.1×10^{11} cm^{-2}, the output power was only ~60 mW for a J_{max} of about 650 A/cm^2. In contrast, for samples grown with Ga1, even with n_s ~5×10^{10} cm^{-2}, output powers of up to 180 mW for a J_{max} of ~620 A/cm^2 could easily be achieved. This trend was not only observed for this active region design, but also for all other QCL active region designs investigated. Beside the output power, the maximum working temperature of the devices grown with Ga1 was higher by more than 15 K (data not shown).

It has been argued previously that the level of impurities in a THz QCL will influence the scattering and unintentional tunneling within the device, as well as affecting the lifetimes of the laser levels and the electron injection efficiency [11]. It is not easy to evaluate quantitatively the microscopic mechanism occurring in THz QCLs, especially the influence of lifetimes on the lasing. However, the global transit time (τ_{trans}) of the electron across a period of the active region at resonance can be experimentally determined [9, 21, 23, 24]. As shown in Fig. 4(b), we observed a significant decrease of τ_{trans} in the QCLs grown with Ga1, which gave far higher performance.

Growth of THz QCLs is both costly and time-consuming, taking over a day per sample. In addition to calibrating the precise thicknesses/compositions of the layers, and achieving growth reproducibility, it can be seen that it is also essential that the material grown is of the highest quality, with low levels of background impurities. In our work, we use unintentionally doped bulk GaAs layers as a technique for assessing the background carrier concentration of the MBE system. In contrast, Beere et al. have used the <4 K mobility of high electron mobility transistors (HEMT) as a gauge to evaluate the material quality, and have correlated this with QCL device performance [11], observing that the higher the electron mobility, the better the performance. This technique does, though, require access to low temperature characterization equipment, and the low-temperature performance of HEMTs is itself strongly dependent both on the device structure and growth conditions. Whether this, or the more straightforward assessment of bulk GaAs, is the better way for setting up an MBE system for QCL growth remains to be determined, but it is clear that some technique needs to be used to maximize the yield of high-performance QCL wafers.

4.3 Effects of device fabrication

Figure 5 shows the dependencies of the measured peak output powers on ridge area (L × w) for as-cleaved devices, fabricated from two different QCL wafers based on M-BTC-RP and MQW-LO designs. The measurements were performed at a heat sink temperature of 10 K. Regardless of the active region design, the device peak output power scales almost linearly with the ridge area. For devices with an M-BTC-RP design, peak output powers of up to ~780 mW were obtained from a single facet (or 1.56 W if it is assumed that the same power is radiated from both facets), whilst for devices from the wafer with an MQW-LO design, peak output power of up to ~375 mW were achieved from a single facet (750 mW from both facets). In principle, further increases in ridge area will lead to even higher output powers. However, there is a trade-off as the heat dissipation also increases.

To increase the emitted power from a single facet further, a high-reflectivity (HR) coating can be applied to the opposite facet [25]. SiO_2(150 nm)/Ti(10 nm)/Au(150 nm)/SiO_2(200 nm), deposited by an electron beam evaporator, was used as HR coating for our work. Figure 6 shows the LIV characteristics of two test devices with, and without, facet coating at 10 K. The maximum peak output power from a single facet increased from 275 mW without HR coating to a maximum of 375 mW with facet coating, corresponding to an increase of ~35%. In addition, with facet coating, there is ~10% decrease in the threshold current density. This can be attributed to the fact that the output power and threshold current density depend on the facet reflectivity through the mirror losses. Using this strategy, we have demonstrated THz QCLs with a peak output power ~1.01 W (at 10 K) from a single facet [6].

4.4 Results of high power devices

Figure 7 shows the typical LIV characteristics as a function of heat sink temperature of two devices with the same dimension of 3 mm × 425 μm. They were fabricated from wafers from different growth campaigns. Taking the total light emitted from both facets into account, maximum peak output powers of up to 1.56 W and 1.34 W at 10 K were obtained. Even at ~77 K, they still delivered peak output powers of ~0.8 W. The devices operated in a frequency range of 3.1 – 3.4 THz (see insets) and with maximum heat-sink temperatures of 123 K and 118 K, respectively. There is a slight discrepancy between the output power levels from these two devices, which probably results from a slightly different injector doping level, as reflected by the different device threshold current densities. Nevertheless, the performance of the two devices is very similar, providing further evidence that run-to-run growth reproducibility can be achieved through careful pre-growth calibration and growth monitoring using pyrometric spectrometry.

5. Conclusion

We have reported the MBE growth and realization of GaAs/AlGaAs THz QCLs with Watt- level optical output powers. This reflects a precise control of layer thickness/alloy composition during growth, a high material quality, and optimized device fabrication. By using pyrometric spectrometry, we demonstrated that precise layer thickness control as well as run-to-run reproducibility of THz QCLs is feasible. We also showed that QCL performance is very sensitive to the background material quality of the GaAs. With appropriate active region design, and optimized injector doping and device fabrication, reproducible high performance devices with total optical output powers of up to 1.56 W from both laser facets were demonstrated.

Acknowledgments

We express our special thanks to Dr I. Farrer (University of Cambridge, UK), Dr S. Y. Zhang (University of Sheffield, UK), Dr F. W. M. van Otten (Eindhoven University of Technology, Netherlands) and Prof. H. Y. Liu (University College London, UK) for their help with x-ray diffraction measurements. We are indebted to Drs J. Freeman, P. Dean, and A. Valavanis, and Ms. R. A. Mohandas (University of Leeds, UK), for their assistance in device measurements. We would also like to thank Dr Jingbo Wu (University of Leeds, UK) for his fruitful discussions. We acknowledge financial support from the EPSRC (UK) 'COTS' programme, the ERC grant 'TOSCA', and the European Space Agency. AGD acknowledges support from the Royal Society and the Wolfson Foundation.

References

1. M. Tonouchi, “Cutting-edge terahertz technology,” Nat. Photonics **1**(2), 97–105 (2007).
2. S. Kumar, “Recent progress in terahertz quantum cascade lasers,” IEEE J. Sel. Top. Quantum Electron. **17**(1), 38–47 (2011).
3. R. Köhler, A. Tredicucci, F. Beltram, H. E. Beere, E. H. Linfield, A. G. Davies, D. A. Ritchie, R. C. Iotti, and F. Rossi, “Terahertz semiconductor-heterostructure laser,” Nature **417**(6885), 156–159 (2002).
4. D. Turčinková, G. Scalari, F. Castellano, M. I. Amanti, M. Beck, and J. Faist, “Ultra-broadband heterogeneous quantum cascade laser emitting from 2.2 to 3.2 THz,” Appl. Phys. Lett. **99**(19), 191104 (2011).
5. S. Fathololoumi, E. Dupont, C. W. I. Chan, Z. R. Wasilewski, S. R. Laframboise, D. Ban, A. Mátyás, C. Jirauschek, Q. Hu, and H. C. Liu, “Terahertz quantum cascade lasers operating up to □□200 K with optimized oscillator strength and improved injection tunneling,” Opt. Express **20**(4), 3866–3876 (2012).
6. L. H. Li, L. Chen, J. X. Zhu, J. Freeman, P. Dean, A. Valavanis, A. G. Davies, and E. H. Linfield, “Terahertz quantum cascade lasers with >1 Watt output powers,” Electron. Lett. **50**(4), 309–311 (2014).
7. B. S. Williams, S. Kumar, Q. Hu, and J. L. Reno, “High-power terahertz quantum-cascade lasers,” Electron. Lett. **42**(2), 89–90 (2006).
8. M. Wienold, L. Schrottke, M. Giehler, R. Hey, W. Anders, and H. T. Grahn, “Low-voltage terahertz quantum cascade lasers based on LO-phonon-assisted interminiband transitions,” Electron. Lett. **45**(20), 1030 (2009).
9. M. Amanti, G. Scalari, R. Terazzi, M. Fischer, M. Beck, J. Faist, A. Rudra, P. Gallo, and E. Kapon, “Bound-to-continuum terahertz quantum cascade laser with a single-quantum-well phonon extraction/injection stage,” New J. Phys. **11**(12), 125022 (2009).
10. S. Kumar, C. W. I. Chan, Q. Hu, and J. L. Reno, “A 1.8-THz quantum cascade laser operating significantly above the temperature of ω/kB,” Nat. Phys. **7**(2), 166–171 (2011).
11. H. E. Beere, J. C. Fowler, J. Alton, E. H. Linfield, D. A. Ritchie, R. Kohler, A. Tredicucci, G. Scalari, L. Ajili, J. Faist, and S. Barbieri, “MBE growth of terahertz quantum cascade lasers,” J. Cryst. Growth **278**(1-4), 756–764 (2005).
12. H. C. Liu, M. Wächter, D. Ban, Z. R. Wasilewski, M. Buchanan, G. C. Aers, J. C. Cao, S. L. Feng, B. S. Williams, and Q. Hu, “Effect of doping concentration on the performance of terahertz quantum-cascade lasers,” Appl. Phys. Lett. **87**(14), 141102 (2005).
13. A. Andrews, T. Roch, A. Benz, G. Fasching, W. Schrenk, K. Unterrainer, and G. Strasser, “Optimization of MBE growth parameters for GaAs-based THz quantum cascade lasers,” AIP Conf. Proc. **893**, 51–52 (2007).
14. T. Roch, A. Andrews, G. Fasching, A. Benz, W. Schrenk, K. Unterrainer, and G. Strasser, “High-quality MBE growth of AlχGa1-χ As-based THz quantum cascade lasers,” Cent. Eur. J. Phys. **5**(2), 244–251 (2007).
15. S. P. Khanna, S. Chakraborty, M. Lachab, N. M. Hinchcliffe, E. H. Linfield, and A. G. Davies, “The growth and measurement of terahertz quantum cascade lasers,” Physica E. **40**, 1859–1861 (2008).
16. Z. R. Wasilewski, “MBE growth of THz quantum cascade lasers,” in Molecular Beam Epitaxy: From Research to Mass Production, M. Henini, ed. (Elsevier Inc., 2013).
17. F. G. Boebel, H. Mijller, B. Hertel, H. Grothe, G. Schraud, St. Schrader, and P. Chow, “In-situ film thickness and temperature control of molecular-beam epitaxy growth by pyrometric interferometry,” J. Cryst. Growth **150**, 54–61 (1995).
18. A. J. SpringThorpe, T. P. Humphreys, A. Majeed, and W. T. Moore, “In situ growth rate measurements during molecular beam epitaxy using an optical pyrometer,” Appl. Phys. Lett. **55**(20), 2138 (1989).
19. W. G. Breiland and K. P. Killeen, “A virtual interface method for extracting growth rates and high temperature optical constants from thin semiconductor films using in situ normal incidence reflectance,” J. Appl. Phys. **78**(11), 6726 (1995).
20. C. H. Kuo, S. Anand, R. Droopad, K. Y. Choi, and G. N. Maracas, “Measurement of GaAs temperature- dependent optical constants by spectroscopic ellipsometry,” J. Vac. Sci. Technol. B **12**(2), 1214 (1994).
21. J. Faist, Quantum Cascade Lasers (Oxford University Press, 2013), Chap. 7.
22. C. Gmachl, F. Capasso, D. L. Sivco, and A. Y. Cho, “Recent progress in quantum cascade lasers and applications,” Rep. Prog. Phys. **64**(11), 1533–1601 (2001).
23. T. Aellen, M. Beck, N. Hoyler, M. Giovannini, J. Faist, and E. Gini, “Doping in quantum cascade lasers. I. InAlAs-InGaAs/InP midinfrared devices,” J. Appl. Phys. **100**(4), 043101 (2006).
24. L. Ajili, G. Scalari, M. Giovannini, N. Hoyler, and J. Faist, “Doping in quantum cascade lasers. II. GaAs/Al0.15Ga0.85As terahertz devices,” J. Appl. Phys. **100**, 043102 (2006).
25. R. Maulini, A. Lyakh, A. Tsekoun, R. Go, C. Pflüg, L. Diehl, F. Capasso, and C. K. N. Patel, “High power thermoelectrically cooled and uncooled quantum cascade lasers with optimized reflectivity facet coatings,” Appl. Phys. Lett. **95**(15), 151112 (2009).

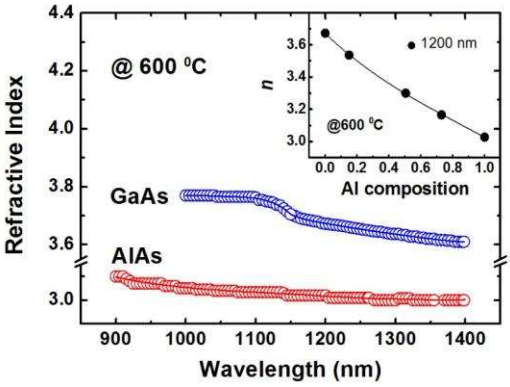

Fig. 1. Refractive index (n) for GaAs and AlAs as a function of wavelength. Inset: the dependence of n on the Al composition in an AlGaAs layer. The solid black circles and line are experimental data and the least fitting curve, respectively.

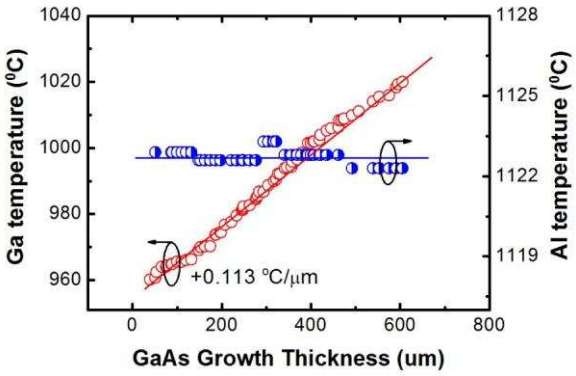

Fig. 2. Typical variation of the gallium cell temperature required to achieve a 1 μm/hour GaAs growth rate as a function of the total thickness of deposited GaAs during a growth campaign. Each data point corresponds to a single wafer growth. The aluminum data reflecting the required cell temperature to achieve a constant growth rate of 0.176 um/hr, as used for the majority of THz QCL growths, are also shown. These aluminum data points correspond to THz QCL growths during the campaign.

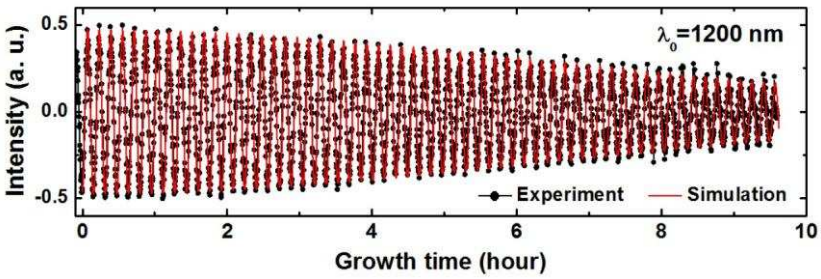

Fig. 3. Typical pyrometric oscillation recorded during growth of a THz QCL structure based on [5] using growth rate compensation. The theoretical simulation assumed a constant G_{QCL} of 1.036 um/hr. No account is made for any shutter transients.

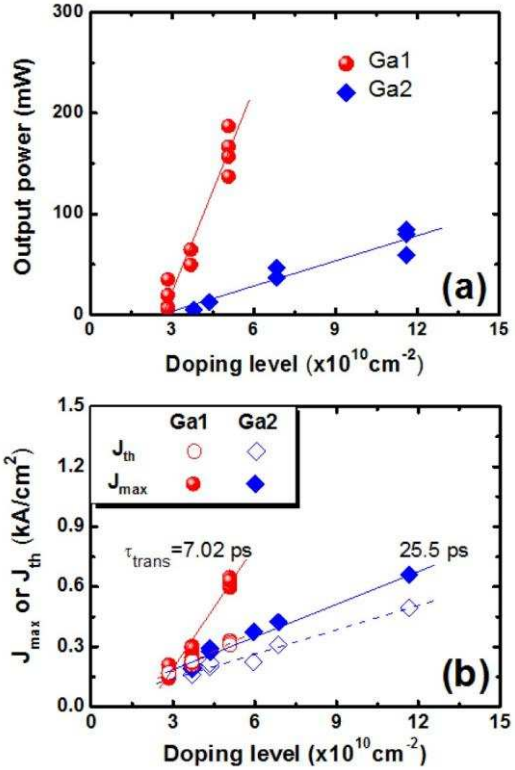

Fig. 4. Variation of (a) peak output power and (b) J_{max} and J_{th} with injector doping level for devices with dimension of 3 mm × 145 µm. The active region (BTC-RP) is based on [9]. Two Ga cells (Ga1, Ga2) were used for these growths. Ga1 had extremely high purity, but Ga2 was known to be contaminated and hence the GaAs was of lower quality. The total net unintentional background doping level from both cells was, however, <2 x 10^{14} cm^{-3} (p-type) – rather less than the intended injector doping levels.

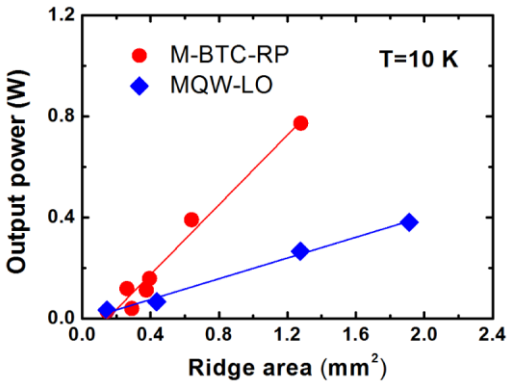

Fig. 5. Dependencies of the measured peak output powers on ridge area (L × w) for as-cleaved devices. The devices were fabricated from two different QCL wafers which have M-BTC-RP and MQW-LO active regions designs. The output powers were recorded from a single facet, and do not include any corrections to account for the measurement system.

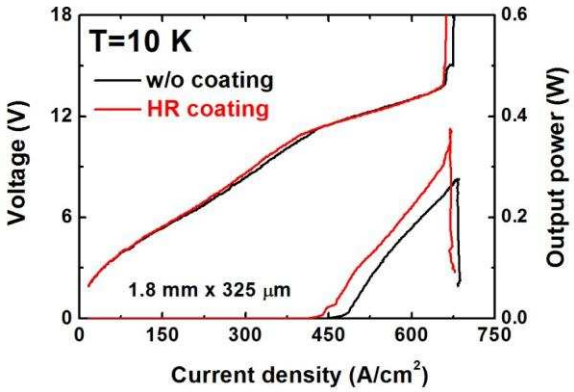

Fig. 6. LIV characteristics of two test devices (1.8 mm × 325 μm) with, and without, facet coating. The active region is based on the M-BTC-RP design. The output power was recorded from the front facet.

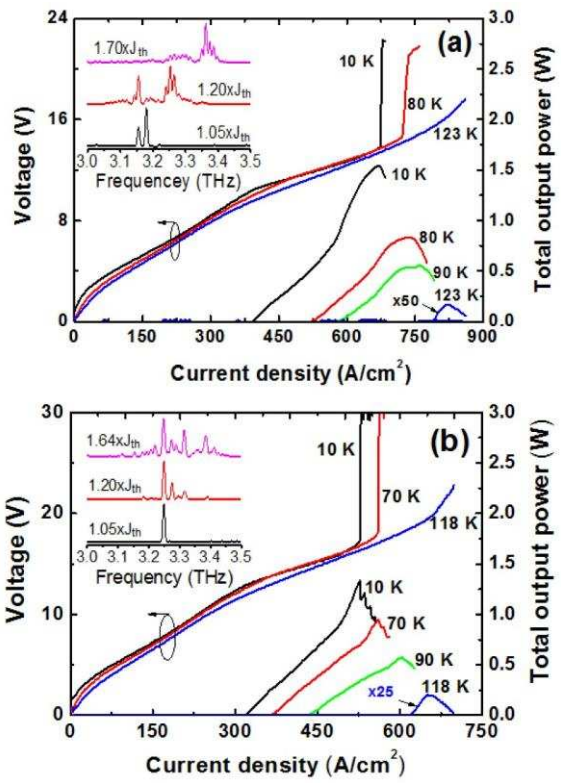

Fig. 7. Typical LIV characteristics of two as-cleaved devices with the same dimension of 3 mm × 425 μm (ridge area of 1.28 mm^2). The devices were fabricated from wafers grown during different growth campaigns, i.e., (a) on May 20, 2013 and (b) on March 11, 2014. The output powers in this figure account for radiation from both laser facets. Insets: lasing spectra for different device current densities at 10 K.